Ion-Beam Induced Luminescence and Damage of Er_2O_3[*)]

Daiji KATO, Hiroyuki A. SAKAUE, Izumi MURAKAMI, Teruya TANAKA,
Takeo MUROGA and Akio SAGARA

*Fusion Systems Research Division, Department of Helical Plasma Research, National Institute for Fusion Science,
322-6 Oroshi-cho, Toki, Gifu 509-5292, Japan*

Ion-beam induced luminescence of sintered Er_2O_3 samples irradiated by Ar^+ ion-beams was measured in a visible range. In this experiment, three emission bands were observed at 500-520, 540-570, and 640-690 nm. The measured luminescence band at 640-690 nm is resolved into Lorentzian Stark component having a $\sim 10^{12}$ Hz width in frequency. Center wavelengths of the Stark components agree with those of intra-4f transitions of Er^{3+} ($4f^{11}$) ions situated at C_2 symmetry cation sites in pure Er_2O_3. However, resonance broadening due to nearby Er^{3+} in the crystal accounts only 1% of the total width. Depopulation of the crystalline oxide in irradiated regions is inferred from decreasing intensity of the emission band at 640-690 nm during continuous irradiation. The emission bands at 500-520 and 540-570 nm still remained in heavily damaged samples look similar with those observed with a metallic Er target.

1. Inroduction

Er_2O_3 electric insulating coating is being developed for reduction of the MHD pressure drop in Li/V-alloy blanket systems [1]. It was demonstrated that the Er_2O_3 coating serves also as a tritium permeation barrier of blanket systems made of other breeder and coolant such as Flibe and Li-Pb [2]. However, neutron damages of the coating in fusion reactors are a big concern. Ion-beam damages are often used to simulate the neutron damages. Changes in crystallinity of the irradiated sample may be inferred from changes in ion-beam induced luminescence spectra, because optical transitions of trivalent Er ions (Er^{3+}) in the Er_2O_3 crystals are known rather strong and sharp [3]. The ground state of Er^{3+} has an incomplete 4f sub-shell ($4f^{11}$). The intra-4f transitions from lower excited states to the ground state are observed as the luminescence in Infrared and visible ranges. Tanaka *et al.* [4] investigated the ion-beam induced visible luminescence of Er_2O_3 coating samples irradiated by 100 keV H^+ and Ar^+ ion-beams at Osaka Univ. The similar measurements have recently been undertaken using an apparatus in NIFS in order to understand relations between the crystallinity and the luminescence spectra. In the present study, the visible spectra of sintered Er_2O_3 samples bombarded by Ar^+ ion-beams were measured.

2. Experimental Apparatus and Method

The experimental apparatus consists of an ion-beam source, a collision chamber, and a CCD spectrometer. The ion source is a part of medium current ion implanter (UL-VAC IM-200MH-FB) used for semiconductor production (Freeman-type) in NIFS [5]. Ion-beam extracted from the Freeman ion source was introduced into the collision chamber after analyzing the mass to charge ratio by a magnet. We could use primary Ar^+ ion beam of about $0.1 \sim 100\,\mu A$ in current at 33, 50, and 70 keV in kinetic energy. In the collision chamber, target samples are set on a grounded movable stage made of stainless steels. The stage can be moved in direction parallel to the ion-beam axis. In the present study, high purity (3N) sintered Er_2O_3 disks ($25\,mm\varphi \times 1\,mm$) provided by TEP Corporation were used as the target sample. Present results in this paper were obtained with the same sample. To the ion-beam axis, the sample surface was leaned 45 degrees and placed (see Fig. 1). An electrode with a hole of 5 mm diameter (collimator) was placed in front of the sample. The electrode surface was biased -100 V to retard secondary electrons from the irradiated sample. Ion-beam current on the target was measured by a Faraday cup installed in between the electrode and the target sample. The Faraday cup was placed out of the ion-beam axis during irradiation on the target. Electric current through the grounded target stage is induced by breakdown of electrical insulation in the irradiated sample. Magnitudes of the induced electric current were about one fifth of the ion-beam current measured by the Faraday cup. In this paper, the ion-beam currents on
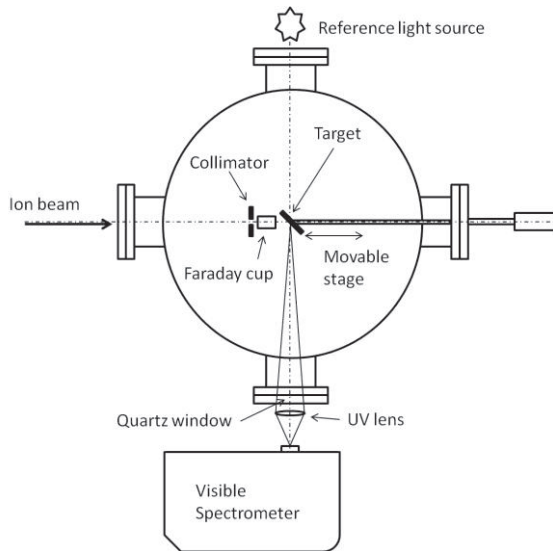
Fig. 1   Schematic illustration of the collision chamber and the visible spectrometer.
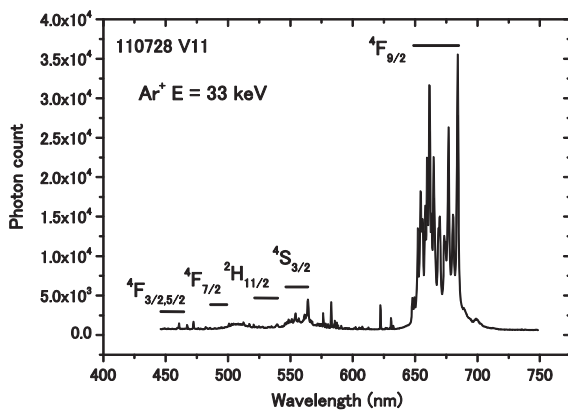

Fig. 2   Measured visible spectrum. The spectrum was obtained using a grating of 300 Grooves/mm. Reflectivity of the grating decreases with the wavelength, and quantum efficiency of the CCD is almost uniform over the whole wavelength range of the present interest.

Fig. 3   High dispersion Stark spectrum of the luminescence band at 640-690 nm. Dash-dotted lines indicate $^{4}F_{9/2}$-$^{4}I_{15/2}$ transition wavelengths of Er^{3+} in the C_2 cation sites of pure Er_2O_3.

Fig. 4   2D image of the ion-beam induced photon emission spectra. (a)-(c) are spectra for sintered Er_2O_3 samples irradiated by 33 keV Ar^+ at 10 µA in current, and (d) for Er disc at 50 µA. These ion-beam currents were measured using the Faraday cup. The spectra (a)-(b)-(c) were measured successively with increment of the ion-beam dose by about 10^{21} m^{-2}.

the target sample are estimated using the induced electric current for spectra shown in Figs. 2 and 3 whereas those were measured using the Faraday cup for spectra in Fig. 4.

After passing through a quartz window and the ultra violet (UV) condenser lens, the light from the target sample is focused onto the entrance slit (30 µm) of a spectrometer equipped with a charge coupled device (CCD). The optical axis crosses with the ion-beam axis and the sample surface at right angle and 45 degree, respectively. H and He discharge tubes were used as the reference light source for wavelength calibration.

3. Result and Discussion

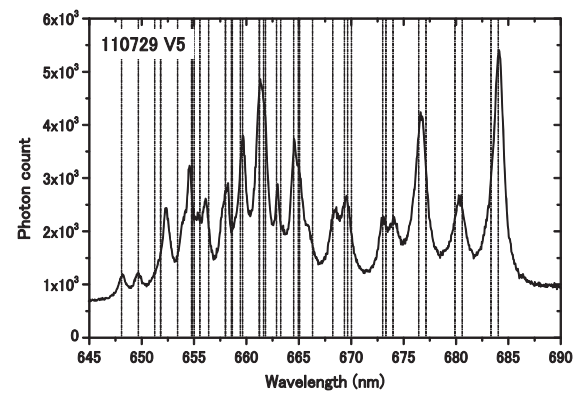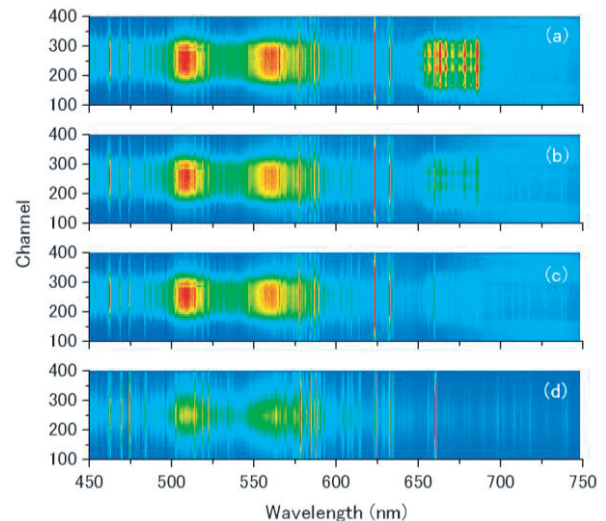Figure 2 shows a photon emission spectrum in a visible range obtained by Ar^+ ion-beams at incident energy of 33 keV. Since measurement of Fig. 2 has been performed before we installed the Faraday cup, we could measure only the induced electrical current (2 µA in this case) through the grounded target stage. Hence, the ion-beam current on the target is estimated about 10 µA. Since ion-beam spot size on the target is about 5 mmφ, Ar^+ ion number density irradiated on the target during the measurement (1 minute exposure) is estimated about 2×10^{20} m^{-2}. Three emission bands were observed in the spectrum at 500-520, 540-570, and 640-690 nm, respectively. Besides the emission bands, narrow emission lines of sputtered neutral Er are superimposed in the spectrum. In the figure, wavelength ranges of Stark bands due to the intra-4f transitions

from $^4F_{9/2,7/2,5/2,3/2}$, $^4S_{3/2}$, and $^2H_{11/2}$ excited states to the ground state, $^4I_{15/2}$, are also indicated by horizontal lines. Stark component of the strongest emission band at 640-690 nm is clearly resolved as seen in Fig.3. The spectrum shown in Fig. 3 was measured with the same ion-beam energy but the ion-beam current of about 15 μA. This ion-beam current is also estimated using the induced electric current, 3 μA, for the same reason with the measurement of Fig. 2. The figure shows the Stark spectrum taken with a higher dispersion grating (1200 Grooves/mm) together with $^4F_{9/2}$-$^4I_{15/2}$ transition wavelengths of Er^{3+} in the C_2 cation sites of pure Er_2O_3 [6]. Perfect agreement with measured wavelengths suggests the emitter for the band at 640-690 nm must be the Er^{3+} ion situated in the C_2 cation sites of the pure Er_2O_3.

Peak of the each Stark component is fitted to the Lorentzian profile of a $\sim 10^{12}$ Hz width in frequency. Since radiative life-times of the $^4F_{9/2}$ state are estimated to be about 500-800 μs [7], the exceedingly broad line width may be ascribed to resonance broadening (self-broadening) by nearby Er^{3+} ions in the crystal. The resonance broadening formula is given by [8],

$$w_r = 3\pi \sqrt{\frac{g_1}{g_2}} \left(\frac{e^2 f}{4\pi\varepsilon_0 m\omega_0} \right) N, \qquad (1)$$

where g's are statistical weights of the upper and the lower Stark levels, m electron mass, f the oscillator strength of the electric-dipole transition, ω_0 the transition frequency, and N the particle number density of the emitter, namely Er^{3+}, e.g. $N = 2.7 \times 10^{28}$/m^3 for perfect crystals. We evaluated the resonance broadening corresponding to an isolated Stark component at 648 nm. The oscillator strength value (5.2×10^{-7}) of doped Er^{3+} ions in Y_2O_3 [9] is adopted in the evaluation. This may presumably not cause large errors, because the crystal structure is the same for both of Y_2O_3 and Er_2O_3. However, it turns out that the resonance broadening accounts only 1% of the total width.

As the ion-beam dose increases, the emission band at 640-690 nm becomes weaker while intensities of the other two bands change little. This is illustrated in Figs. 4 (a)-(c). Figure 4 (d) shows the emission spectrum with a metallic Er target for comparison. The 2-dimensional images show spatial distributions of the emission spectra along vertical direction to the ion-beam axis and the line-of-sight. The band emissions are strong in the beam-spot on the target whereas narrow line emissions have broader distributions along the vertical direction suggesting that the emitters are sputtered particles out of the target surface. Inhomogeneous spatial distribution of the emission band at 640-690 nm may indicate distribution of crystalline Er_2O_3 in the irradiated sample. Apparently smooth distribution of the other two emission bands at 500-520 nm and 540-570 nm corresponds probably to an ion-beam profile, which indicates uniform distribution of emitters on the target. It is noted that the similar band emissions are observed also in the Er spectrum (Fig. 4 (d)). Thus, the emitters asso-

ciated to the two bands must be different from the Er^{3+} ions in the crystalline oxides. The ion-beam irradiation on the same sample was performed again after the ion-beam was stopped for a while, however the band emission at 640-690 nm is not recovered afterwards. Figure 4, therefore, depicts that by the ion-beam irradiation populations of the crystalline oxides in the irradiated region become smaller irreversibly.

SRIM code [10] simulation of ion-induced damages was performed assuming amorphous targets with stoichiometric mixture ratio of Er_2O_3. The simulation gives totally 432 displacements distributed to depth of 60 nm and about 8 sputtered atoms per incident Ar^+ ion at 33 keV. This result suggests substantial damages and changes of chemical compositions in the irradiated surface layers. Preferential sputtering of O may form metallic Er layers on the surface. This plausible speculation supports the apparent similarity of the damaged oxides spectrum and the Er spectrum, although mechanisms of the band emissions at 500-520 nm and 540-570 nm with the Er target are still to be resolved. It is also noteworthy that the spectrum in Fig. 2 is dominated by the emission band of the crystalline oxides at 640-690 nm. Since the measurements of Figs. 2 and 3 have been performed before those of Figs. 4 (a)-(c), accumulated ion dose (damage level) of the sample used in the former measurement is much lower than those used in the latter.

4. Summary

The ion-beam induced photon emissions were measured in a visible range of 450-750 nm for sintered Er_2O_3 samples by Ar^+ ions at 33 keV. Three emission bands at 500-520, 540-570, and 640-690 nm were observed. The emission band at 640-690 nm is clearly identified as $(4f^{11})$ $^4F_{9/2}$-$^4I_{15/2}$ transition of trivalent Er^{3+} ions in the C_2 cation sites of pure Er_2O_3 crystals. Preliminary analysis, however, revealed that the resonance broadening seems insufficient to explain exceedingly broad Lorentzian width of the Stark component in the emission band. Intensity of the emission band at 640-690 nm decreases substantially during continuous ion-beam irradiation, which indicates depopulation of the crystalline oxide in the irradiated region. Dose dependence of the emission spectra suggests formation of metallic Er layers on the surface of heavily damaged samples. For a better understanding, surface structures and elemental compositions are investigated in future studies.

[1] T. Muroga *et al.*, J. Nucl. Mater. **367-370**, 780 (2007).
[2] D. Levchuk *et al.*, J. Nucl. Mater. **367-370**, 1033 (2007).
[3] A. Polman, J. Appl. Phys. **82**, 1 (1997).

[4] T. Tanaka *et al.*, J. Nucl. Mater. **417**, 794 (2011).

[5] K. Motohashi *et al.*, *Plasma Conference 2011* (Kanazawa, 2011) 22P174-B.

[6] J.B. Gruber *et al.*, J. Appl. Phys. **108**, 023109 (2010).

[7] M.J. Weber, Phys. Rev. **171**, 283 (1968).

[8] H.R. Griem, *Plasma Spectroscopy* (McGraw-Hill, New York, 1964) p. 95.

[9] C.A. Morrison *et al.*, J. Chem. Phys. **79**, 4758 (1983).

[10] J.F. Ziegler, J.P. Biersack and U. Littmark, *The Stopping and Range of Ions in Solids* (Pergamon Press, New York, 1985).